



**HAL**  
open science

## Preclinical characterization of alginate-Poly-L-Lysine encapsulated HepaRG for extracorporeal liver supply

Mattia Pasqua, Ulysse Pereira, Claire de Lartigue, Jonathan Nicolas, Pascale Vigneron, Quentin Dermigny, Cécile Legallais

### ► To cite this version:

Mattia Pasqua, Ulysse Pereira, Claire de Lartigue, Jonathan Nicolas, Pascale Vigneron, et al.. Preclinical characterization of alginate-Poly-L-Lysine encapsulated HepaRG for extracorporeal liver supply. *Biotechnology and Bioengineering*, 2021, 118 (1), 10.1002/bit.27583 . hal-02961888

**HAL Id: hal-02961888**

**<https://hal.science/hal-02961888>**

Submitted on 11 Dec 2020

**HAL** is a multi-disciplinary open access archive for the deposit and dissemination of scientific research documents, whether they are published or not. The documents may come from teaching and research institutions in France or abroad, or from public or private research centers.

L'archive ouverte pluridisciplinaire **HAL**, est destinée au dépôt et à la diffusion de documents scientifiques de niveau recherche, publiés ou non, émanant des établissements d'enseignement et de recherche français ou étrangers, des laboratoires publics ou privés.



**Preclinical characterization of alginate-Poly-L-Lysine encapsulated HepaRG for extracorporeal liver supply**

Journal:	<i>Biotechnology and Bioengineering</i>
Manuscript ID	Draft
Wiley - Manuscript type:	Article
Date Submitted by the Author:	n/a
Complete List of Authors:	<p>Pasqua, Mattia; Universite de Technologie de Compiegne, CNRS, Biomechanics &amp; Bioengineering          Pereira, Ulysse; Universite de Technologie de Compiegne, CNRS, Biomechanics &amp; Bioengineering          de Lartigue, Claire; Universite de Technologie de Compiegne, CNRS, Biomechanics &amp; Bioengineering          Nicolas, Jonathan; Universite de Technologie de Compiegne, CNRS, Biomechanics &amp; Bioengineering          Vigneron, Pascale; Universite de Technologie de Compiegne, CNRS, Biomechanics &amp; Bioengineering          Dermigny, Quentin; Universite de Technologie de Compiegne, CNRS, Biomechanics &amp; Bioengineering          Legallais, Cecile; Université de Technologie de Compiègne, CNRS, Biomechanics &amp; Bioengineering; Hôpital Paul Brousse, DHU Hepatinov, Centre Hépatobiliaire</p>
Key Words:	Acute liver failure, Bioartificial liver, Liver tissue engineering, Bioreactor, Organoid

SCHOLARONE™  
Manuscripts

**Title:**

Preclinical characterization of alginate-Poly-L-Lysine encapsulated HepaRG for extracorporeal liver supply

**Authors and affiliations:**

Mattia Pasqua,<sup>a</sup> Ulysse Pereira,<sup>a</sup> Claire de Lartigue,<sup>a</sup> Jonathan Nicolas,<sup>a</sup> Pascale Vigneron,<sup>a</sup> Quentin Dermigny,<sup>a</sup> Cécile Legallais.<sup>a,b</sup>

<sup>a</sup>UMR CNRS 7338 Biomechanics & Bioengineering, Université de technologie de Compiègne, Sorbonne Universités, Rue du Dr Schweitzer, 60203 Compiègne, France.

<sup>b</sup>DHU Hépatinoy, 12 Avenue Paul Vaillant Couturier, 94800 Villejuif, France.

E-mail addresses and telephone numbers: mattia.pasqua@utc.fr (Mattia Pasqua) +33 3 44 23 44 23, ulysse.pereira@utc.fr (Ulysse Pereira) +33 3 44 23 44 23, claire.de-lartigue@utc.fr (Claire de Lartigue) +33 3 44 23 44 23, jonathan.nicolas@etu.utc.fr (Jonathan Nicolas) + 33 3 44 23 44 23, pascale.vigneron@utc.fr (Pascale Vigneron) +33 3 44 23 44 23, quentin.dermigny@utc.fr (Quentin Dermigny) + 33 3 44 23 44 23, cecile.legallais@utc.fr (Cécile Legallais) +33 3 44 23 44 23.

**Corresponding author:**

Cecile Legallais (cecile.legallais@utc.fr), +33 3 44 23 44 23

UMR CNRS 7338 Biomechanics & Bioengineering, Université de technologie de Compiègne, Alliance Sorbonne Université, Rue du Dr Schweitzer, 60203 Compiègne, France

**Abstract**

We recently demonstrated that HepaRG cells encapsulated into 1.5% alginate beads are capable of self-assembling into spheroids. They adequately differentiate into hepatocyte-like cells, with hepatic features observed at day 14 post-encapsulation required for external bioartificial liver applications. Preliminary investigations performed within a bioreactor under shear stress conditions and using a culture medium mimicking acute liver failure (ALF) highlighted the need to reinforce beads with a polymer coating. We demonstrated in a first step that a Poly-L-Lysine coating improved the mechanical stability, without altering the metabolic activities necessary for bioartificial liver applications (such as ammonia and lactate elimination). In a second step, we tested the optimized biomass in a newly-designed perfused dynamic bioreactor (PDB), in the presence of the medium model for pathological plasma for 6 hours. Performances of the biomass were enhanced as compared to the steady configuration, demonstrating its efficacy in decreasing the typical toxins of ALF. This type of bioreactor is easy to scale up as it relies on the number of micro-encapsulated cells, and could provide an adequate hepatic biomass for liver supply. Its design allows it to be integrated into a hybrid artificial/bioartificial liver setup for further clinical studies regarding its impact on ALF animal models.

**Graphical abstract****Keywords**

Acute liver failure, bioartificial liver, liver tissue engineering, bioreactor, organoid

## 1. Introduction

Acute liver failure (ALF) is a devastating syndrome involving severe injury to liver cells. It affects previously healthy individuals, and has a frequently fatal outcome (Keeffe, 2005). Following diagnosis of ALF, the optimal treatment is orthotopic liver transplantation (OLT) needed within a few days, making the availability of donor organs far lower than the demand (Van De Kerkhove et al., 2005). It is therefore urgent to develop new approaches capable of improving the management of ALF. In this sense, artificial livers (ALs) have been proposed as temporary therapy with purely detoxification functions. However, while analysis of clinical studies showed improvements in patients' clinical pictures, there was no such improvement in their survival (Kandiah & Subramanian, 2019). On the other hand, bioartificial livers (BALs) also provide metabolic and synthetic activities, which could better replace the liver functions as extracorporeal therapy. The main goal of this therapy is either to allow the self-regeneration of the diseased liver, thus avoiding OLT and its long-term complications, or to serve as a bridge until a donor organ becomes available.

In the context of BALs, the bioreactor represents one of the key components as it hosts the active biomass. In general, a bioreactor is a volume where biochemical and biological processes take place (Catapano, G., Gerlach, 2007). A bioreactor should provide cells with adequate amounts of oxygen and nutrients, favour mass transfer between cells and fluids (the blood or plasma of the patient in ALF), and support the maintenance of cell viability and functions. To meet these requirements, the best option consists in designing a system in which convection (i.e. flux) from and to the plasma or surrounding medium takes place. Nevertheless, direct contact and shear stress may be harmful to the cells. Encapsulation of the biomass in semi-permeable hollow fibres or porous beads is thus often adopted so as to protect it from the hydrodynamic shear stress imposed by the flux (Rebelo et al., 2015) while simultaneously preserving cell activity (Pasqua et al., 2020), and promoting cell-cell interaction, thus enhancing hepatic-specific functions (Elkayam, Amitay-Shaprut, Dvir-Ginzberg, Harel, & Cohen, 2006).

The fluidized bed bioreactor hosting alginate beads previously developed in our group (Doré & Legallais, 1999) appeared to be a promising design and has been successfully driven to preclinical

1  
2  
3 studies by others (Selden et al., 2017; Zhou et al., 2016) with HepG2 cells or primary porcine  
4  
5 hepatocytes. However, with a very active biomass, such as HepaRG spheroids (6), we recently  
6  
7 observed a phenomenon of severe deterioration of the alginate beads in the bioreactor, when they were  
8  
9 exposed to a human equivalent pathological plasma medium (containing some ALF toxins), leading to  
10  
11 an unacceptable loss of biomass and the associated risk of cells' release to the patient. This  
12  
13 phenomenon has already been noted by other authors (Simó, Fernández-Fernández, Vila-Crespo,  
14  
15 Ruipérez, & Rodríguez-Nogales, 2017) and was attributed to the presence of  $\text{Ca}^{2+}$  chelators (such as  
16  
17 lactate) or anti-gelling cations ( $\text{Na}^+$  and  $\text{Mg}^{2+}$ ) in the surrounding media. For safety reasons,  
18  
19 reinforcement of the alginate beads by means of an external coating becomes essential when using  
20  
21 encapsulated HepaRG or other very active hepatocyte constructs in view of clinical application.  
22  
23

24  
25 Several types of coatings have been proposed to date in the literature (De Vos, De Haan, & Van  
26  
27 Schilfgaarde, 1997; Edwards-Lévy & Lévy, 1999; Joly et al., 1997; Simó et al., 2017). They are often  
28  
29 developed to formulate capsules, whose core is liquid in contrast to beads. These techniques involve  
30  
31 either ionic or covalent (Dusseault et al., 2005; Lou et al., 2017; Simó et al., 2017) interactions  
32  
33 between the surface of the alginate gel and the coating materials. In particular, ionic cross-linking  
34  
35 coating of the beads can be performed thanks to the alginate's ability (with a negatively charged  
36  
37 surface) to form strong electrostatic complexes with polycations (Simó et al., 2017). Of the latter, the  
38  
39 natural polymers Poly-L-lysine (PLL) and Poly-L-ornithine (PLO) are most frequently used to  
40  
41 reinforce the mechanical stability of the alginate beads (Bhujbal, Paredes-Juarez, Niclou, & de Vos,  
42  
43 2014; Du & Yarema, 2014; Goosen, O'Shea, Gharapetian, Chou, & Sun, 1985; Simó et al., 2017).  
44  
45 However, to our knowledge, it has never been applied in the context of an external bioartificial liver  
46  
47 application. On the other hand, an external coating modifies the permeability of the beads without  
48  
49 heavily affecting the cells' metabolic performances and viability, as observed by Capone et al. using  
50  
51 encapsulated HepG2/C3A in alginate-PLL beads (Capone et al., 2013).  
52  
53

54  
55 Therefore, in this study we proposed analysing the impact of a PLL coating on alginate beads'  
56  
57 physical and mechanical properties, and its role on encapsulated HepaRG cells' metabolic  
58  
59 performances. The encapsulated biomass was then transferred to a perfused bioreactor to mimic  
60

1  
2  
3 clinical therapy, demonstrating the features necessary for clinical use of BAL, in terms of cell  
4  
5 metabolic activity and therapy safety.

## 7 **2. Materials and Methods**

### 9 2.1. 2D HepaRG cell culture

11 HepaRG cells from Biopredic (Rennes, France) were expanded into two-dimensional (2D) monolayers  
12 following the indications given by the supplier. The cells were passaged every 2 weeks until passage  
13 18, with HepaRG proliferation culture medium (William's E-WE-, with sodium bicarbonate, without  
14 L-glutamine and phenol red, Sigma-Aldrich, with added Biopredic 710 proliferation media)  
15 replenished three times a week. The cultures were maintained in a humidified environment at 37 °C, 5  
16 % CO<sub>2</sub>. Cells were then detached with trypsin-EDTA 0.25 % (ThermoFisher scientific) from the  
17 culture flasks and used for the encapsulation process.  
18  
19

### 21 2.2. Alginate microencapsulation and PLL coating

22 The cells were mixed in sodium alginate (Manucol-LKX from FMC BioPolymer, Gularonic /  
23 Mannuronic ratio 30-70, viscosity Cps(1 %) 60-170) 1.5 % (w/v), sterilized with successive filtrations  
24 (0.8, 0.45, and 0.22 µm pore size membrane filters). The encapsulation was performed using a home-  
25 made system based on a coaxial airflow extrusion method (Gautier et al., 2011). Briefly, the alginate  
26 solution (1mL) containing cells (5 million) was rapidly extruded through a 24 G nozzle and the  
27 droplets fell into a gelation bath (NaCl 154 mM, HEPES 10 mM, CaCl<sub>2</sub> 115 mM, pH 7.4). This small  
28 volume ensured both even distribution of the cells throughout the beads and the absence of empty  
29 beads. The droplets produced were left to settle for 15 min in the gelation bath to ensure gel formation.  
30 Then, the microbeads were washed three times in WE medium and resuspended in HepaRG  
31 proliferation culture medium. At day 1 post-encapsulation, a PLL coating (Poly-L-lysine  
32 hydrobromide, molecular weight 30,000-70,000, Sigma-Aldrich) was added to the beads, relying on  
33 the protocol developed by Khanna et al. (Khanna, Larson, Moya, Opara, & Brey, 2012) with few  
34 modifications. Briefly, alginate beads containing cells were washed three times in WE medium,  
35 resuspended in a 0.1 % PLL solution and then transferred to culture dishes in continuous orbital  
36 shaking (60 rpm), for 30 minutes. After that, the beads were washed again 3 times with WE medium.  
37 Finally, they were incubated with proliferation culture medium and transferred to culture dishes in  
38  
39  
40  
41  
42  
43  
44  
45  
46  
47  
48  
49  
50  
51  
52  
53  
54  
55  
56  
57  
58  
59  
60

1  
2  
3 continuous orbital shaking in a humidified environment at 37 °C, 5 % CO<sub>2</sub> until day 14. The HepaRG  
4 proliferation culture medium was replaced every 2 days.

### 7 2.3. Culture setups and experimental design

9 The hepatic biomass was tested in two different culture conditions (shaken and perfused), shown in  
10 Figure 1A. Experiments designed to assess the cells' metabolic performance are detailed in Figure 1B.  
11  
12 At the end of each experiment, microbeads were recovered and assessed for cell viability. The quantity  
13 of marker analysed was calculated and normalized by the number of hours of incubation and the  
14 number of cells seeded. Moreover, in order to avoid artefacts, all the metabolic activities tested were  
15 normalized by the quantity present at time zero and by carrying out controls with empty microbeads.  
16  
17 Any influence of the empty beads on the cellular activities assessed was therefore corrected during  
18 analysis of the results.  
19  
20  
21  
22  
23  
24  
25

## 26 **Figure 1**

### 28 2.4. Viability, metabolic and xenobiotic tests

#### 30 2.4.1. Cell viability

32 Aliquots of encapsulated cells were collected and a Live/Dead assay was performed following the  
33 manufacturer's instructions (Invitrogen™LIVE/DEAD™ Viability/Cytotoxicity Kit, for mammalian  
34 cells, ThermoFisher). The nuclei were stained with Hoechst33342 dye (3 μM). The encapsulated cells  
35 were visualized by confocal microscopy.  
36  
37  
38  
39

#### 41 2.4.2. Albumin synthesis

43 Albumin synthesis was quantified using the ELISA test (Human Albumin ELISA kit, Bethyl  
44 Laboratories, Inc.). Analyses were performed in conformity with the manufacturer's instructions.  
45  
46

#### 47 2.4.3. ICG assay

49 The indocyanine green (ICG, Sigma-Aldrich) assay was carried out as previously described (Pasqua et  
50 al., 2020). Briefly, beads were incubated with ICG 1 mg/mL in proliferation culture medium for 30  
51 minutes at 37 °C and 5 % CO<sub>2</sub> to favour the uptake of ICG by the transporters OATP1B3 (solute  
52 carrier organic anion transporter family member 1B3) and NTCP (sodium/taurocholate co-  
53 transporting-polypeptide) (Graaf et al., 2011). ICG was then removed by washing with WE five times  
54 and the microbeads were incubated with proliferation culture medium for 1 hour to study the release of  
55  
56  
57  
58  
59  
60

1  
2  
3 ICG by the transporters MDR3 (multidrug-resistance protein 3) and MRP2 (multidrug-resistance-  
4 associated protein 2) (Cusin et al., 2017). The quantity of ICG released was obtained by measuring its  
5 absorbance (at 820 nm) based on a standard curve generated from a solution containing ICG 1 mg/mL.  
6  
7

#### 8 9 2.4.4. EROD assay

10  
11 The activity of the cytochrome P450-1A1/2 (CYP1A1/2) was studied with the ethoxyresorufin-O-  
12 deethylase (EROD) assay as previously described (Diaz, 2000; Pasqua et al., 2020). The microbeads  
13 were incubated in ethoxyresorufin (10  $\mu$ M), prepared in WE, for 1 hour at 37°C. The substrate  
14 included salicylamide (3 mM) + dicumarol (40  $\mu$ M) in order to inhibit phase II enzymes. The substrate  
15 was converted into resorufin then measured in the supernatant by spectrometry (excitation wavelength  
16 of 535 nm and emission wavelength of 595 nm, Spectafluor Plus, TECAN). The standard curve was  
17 generated with a solution containing exogenous resorufin (10  $\mu$ M).  
18  
19  
20  
21  
22  
23  
24  
25

#### 26 2.4.5. Ammonia and lactate quantification

27  
28 Supernatants of test medium and pathological plasma medium were collected and analysed with  
29 Indiko™ (Thermofisher) to determine the concentration of ammonia and Lactate Assay Kit (Sigma-  
30 Aldrich) to measure the concentration of lactate, following the indications reported by the supplier.  
31  
32  
33

### 34 2.5. Physical and mechanical characterization of empty alginate microbeads

#### 35 36 37 2.5.1. PLL distribution in the alginate beads

38  
39 In order to visualize the distribution of the PLL on the empty alginate beads (i.e. without cells,  
40 produced using the same protocol previously presented), PLL staining with rhodamine was performed.  
41 Firstly, we prepared an NHS-Rhodamine (Thermofisher) solution in DMSO at concentration 50  
42 mg/mL and a solution of sodium bicarbonate at 8.3 mg/mL in double distilled H<sub>2</sub>O, pH 8.2. PLL was  
43 solubilized in the sodium bicarbonate solution at a final concentration of 0.1 %w/v, containing NHS-  
44 Rhodamine solution at a final concentration of 500  $\mu$ g/mL. In order to favour the conjugation between  
45 the NHS-Rhodamine and epsilon-NH<sub>2</sub> of lysine residues, the solution was incubated in the dark for 3  
46 hours at room temperature. The control solution did not contain PLL. After that, the PLL coating was  
47 achieved by putting the beads in contact with this solution, according to the protocol already  
48 described. The beads were finally washed 3 times in DPBS and visualized by confocal microscopy.  
49  
50  
51  
52  
53  
54  
55  
56  
57  
58  
59  
60 The thickness of the external coating was measured using ImageJ 1.52h software.

### 2.5.2. Mechanical characterization

The elastic modulus of the outer surface of the empty beads was measured by microindentation (ChiaroOptics 11, Amsterdam, Netherlands). The probes used for surface indentation had a radius of around 25  $\mu\text{m}$  and a spring constant of 0.5 N/m and 5 N/m, for pure alginate beads and PLL coated ones, respectively. Before testing, the optical sensitivity and the geometrical factor were calibrated by indenting a hard surface (e.g. glass slide). Alginate beads were deposited on a glass slide and then immersed in proliferation culture medium. The probe was placed in contact with a single bead and a maximal indentation of 3  $\mu\text{m}$  was applied. All experiments were performed at room temperature. For each condition, about 15-20 curves (load vs indentation depth) were acquired. Data were analysed using DataViewer 2.2 software (Optics 11, Amsterdam, Netherlands) and the Hertzian theory, which provided the elastic modulus of the indented area.

### 2.5.3. Bead permeability

The permeability of empty alginate beads, with and without a PLL coating, was studied by putting them in contact with fluorescent molecules of different molecular weights and sizes on day 13 post-encapsulation process, in orbital agitation. On day 14, the beads were washed once in WE medium and visualized using confocal microscopy.

## Table 1

### 2.6. Statistical analysis

All the results presented were obtained from at least three independent cultures ( $N \geq 3$ ). The statistical analysis was performed using GraphPad InStat v.3.10. Unpaired data were subjected to a Mann Whitney test or Dunn's Multiple Comparisons Test, with a 95 % confidence level considered significant. P values are presented as follows: no stars:  $p > 0.05$ ; \*\* $p < 0.01$ ; \*\*\* $p < 0.001$ .

## 3. Results

### 3.1. Physical and mechanical characterization of the PLL coated beads

This step was performed with empty beads that were produced following the same protocol as that exposed in the Materials & Methods section for cell encapsulation.

#### 3.1.1. PLL coating and distribution around the alginate beads

1  
2  
3 On day 1, after PLL coating, a variation in the sphericity of the beads was visible (Figure 2A), due to a  
4  
5 shrinking effect. The diameter of the beads decreased by about 20 %, from  $949 \pm 49 \mu\text{m}$  post-  
6  
7 encapsulation to  $785 \pm 25 \mu\text{m}$  after PLL coating. The diameter of the beads, with or without a PLL  
8  
9 coating, then remained stable until the end of the experiment.  
10

11  
12 Phase contrast and confocal microscopy clearly showed that PLL was distributed only on the surface  
13  
14 of the alginate beads, causing a slight morphological variation on their periphery (Figure 3). The  
15  
16 thickness of the external coating was around  $14.4 \pm 6.4 \mu\text{m}$ .  
17

### 18 19 3.1.2. Mechanical properties of the PLL layer

20  
21 The mechanical properties of the surface of single empty beads were assessed by microindentation.  
22  
23 The results showed a significant increase in the elastic modulus of the external area of the beads  
24  
25 coated with PLL, 6.6 times higher in comparison with the pure alginate condition (Figure 2B),  
26  
27 ensuring surface mechanical reinforcement and thus better stability.  
28

### 29 30 **Figure 2**

### 31 32 3.1.3. Bead permeability

33  
34 The porosity of empty alginate beads with or without a PLL coating was evaluated by means of  
35  
36 exposure to different fluorescent markers of increasing size (Table 1). The microscope observations  
37  
38 (Figure 3) did not show any measurable differences between either condition. Albumin, IgG, and  
39  
40 41nm diameter NPs were able to penetrate the core of the beads. Larger NPs were fully retained  
41  
42 entirely outside the beads, and did not colour their inner part green. The cut-off threshold for both  
43  
44 conditions was thus between 41nm and 103nm.  
45

### 46 47 **Figure 3**

### 48 49 3.2. Viability of encapsulated cells over 14 days

50  
51 The production of alginate beads with homogeneous cell distribution was achieved with success and  
52  
53 no empty beads were visible after the cell encapsulation process. We estimated approximately 1100  
54  
55 beads per encapsulation batch (1 mL of alginate solution) by counting them with the optical  
56  
57 microscope. As the initial biomass was 5 million cells/mL of alginate, we calculated approximately  
58  
59  
60

1  
2  
3 4500 cells per bead. As previously observed on empty beads, the PLL coating provoked a shrinking  
4  
5 effect of about 20 % in the diameter of the beads.  
6  
7

8  
9 The number of viable hepatocytes (Figure 4, in green) within the microbeads remained high over time,  
10  
11 as very few dead cells (Figure 4, red stained nuclei) were observed, in comparison with the negative  
12  
13 control where cells were killed by ethanol 70 % exposure. The PLL coating did not seem to affect cell  
14  
15 viability. Therefore, neither the long-time culture nor the coating process had any significant impact  
16  
17 on cellular viability. Qualitatively from day 1 to day 14, a phenomenon of cell-cell aggregation likely  
18  
19 occurred, visible through the incorporation of Calcein-AM by living cells. We observed very similar  
20  
21 results in beads without a PLL coating (data not shown). It should be noted that, once the PLL coating  
22  
23 was present, the beads became opaque making the encapsulated cells difficult to visualize under the  
24  
25 light microscope.  
26

#### 27 **Figure 4**

28  
29 Albumin production is considered to be a quality marker for the hepatic biomass in a bioreactor (Van  
30  
31 Wenum et al., 2014). We therefore evaluated the secretion rate of albumin in order to quantitatively  
32  
33 determine biomass functionality over the 14 days of culture (Figure 1, Supplementary data). Albumin  
34  
35 secretion rate increased from  $0.20 \pm 0.09$  and  $0.17 \pm 0.05$   $\mu\text{g}/\text{h}/10^6$  at day 1 for the conditions without  
36  
37 and with PLL respectively, to  $0.49 \pm 0.15$  and  $1.01 \pm 0.21$   $\mu\text{g}/\text{h}/10^6$  at day 14. This increase was  
38  
39 significant for the two weeks of culture ( $p < 0.01$ ) when the PLL coating was present.  
40  
41

#### 42 3.3. Metabolic activity of cells on day 14

43  
44 To investigate the impact of the PLL coating on the cells' metabolic performance, we designed culture  
45  
46 media with increasing complexity in their composition (Table 2), in order to progressively mimic a  
47  
48 clinical condition of ALF human plasma.  
49

#### 50 **Table 2**

51  
52 The first batch of encapsulated cells was first evaluated in the proliferation culture medium (Table 3).  
53  
54 In the presence of the PLL coating, there was a slight tendency for metabolic activities to decrease, but  
55  
56 this was only significant for CYP1A1/2, 3.5 times lower ( $p < 0.01$ ). However, even in the presence of a  
57  
58 PLL coating, the cells remained metabolically active.  
59  
60

**Table 3**

The same biomass was then used in test medium (Table 3) to measure the rate of albumin production, and the ability of cells to detoxify typical ALF toxins (ammonia and lactate elimination rates). The metabolic activities measured remained equivalent between both conditions (PLL coated vs uncoated).

The second batch of biomass was tested on the equivalent pathological plasma medium, cultivating encapsulated cells in shaken culture and in a perfused dynamic bioreactor (PDB), the biological component of the BAL developed in our laboratory. The aim was to compare the two culture setups and above all to reproduce BAL therapy, using an ALF-human plasma model and a perfusion system. Only the condition “alginate beads with PLL coating” could be exploited with this medium, as without PLL we observed severe bead deterioration.

Importantly, before testing in an equivalent pathological medium, the biomass was exposed to an equivalent plasma medium (HepaRG proliferation culture medium supplemented with 70 g/L bovine serum albumin-BSA-, to mimic healthy human plasma in a total protein concentration), in order to reproduce the BAL priming with a view to clinical therapy. After that, cells were exposed to the equivalent pathological plasma medium for 6 hours.

The ability of the cells to produce albumin and detoxify these toxins is shown in Figure 5. While the albumin secretion rate (Figure 5A) was favoured in the shaken culture, ammonia detoxification (Figure 5B) and lactate clearance rates (Figure 5C) were stronger in the PDB setup.

**Figure 5**

At the end of the experiments, we evaluated the cell viability for both batches of cells. Viability remained high and stable overall for all conditions (Figure 2, Supplementary data). As previously mentioned, a phenomenon of cell-cell aggregation inside the beads was observed.

**4. Discussion**

We recently demonstrated the benefits of using HepaRG cells, capable of differentiating into hepatocyte-like cells (Cerec et al., 2007), encapsulated in alginate beads as the biomass for BAL (Pasqua et al., 2020). The present study therefore focused on the transfer of this biomass within a

1  
2  
3 bioreactor compatible with BAL therapy. However, during the first experiments carried out in an  
4 ALF-human equivalent pathological plasma medium, we observed severe and unacceptable  
5 deterioration of the beads. We thus highlighted the need to reinforce the mechanical properties of the  
6 biomaterial.  
7  
8  
9

10  
11  
12 We hypothesized that the deterioration was due to the presence of an excess of BSA and lactate in the  
13 surrounding medium, both capable of sequestering calcium ions involved in the formation of the  
14 alginate gel. A similar deterioration effect was observed by Benson et al. (Benson, Papas,  
15 Constantinidis, & Sambanis, 1997). In the literature, a PLL coating has been proposed to increase the  
16 structural stability of alginate beads and to limit access of the immune system to the beads/capsules  
17 (Benson et al., 1997; Capone et al., 2013; Berit L. Strand, Coron, & Skjak-Braek, 2017). For this  
18 specific application, if PLL was not additionally coated with a layer of alginate (i.e. alginate-PLL-  
19 alginate beads), it demonstrated immunogenicity (Berit L. Strand et al., 2017) and caused fibrotic  
20 overgrowth when implanted in mice (B. L. Strand et al., 2001). While this additional layer of alginate  
21 on the PLL coating appeared essential for implantation of the encapsulated cells, this is not the case  
22 for extracorporeal circulation devices such as BAL therapy. In fact, most BAL devices, including the  
23 one developed in our laboratory (Figaro, Pereira, Dumé, et al., 2015), include a plasma filter to  
24 separate the plasma from the elements formed of the blood. As a result, the cells of the immune system  
25 are discarded upstream, before making contact with the therapeutic biomass, making activation of a  
26 specific immune response unlikely.  
27  
28  
29  
30  
31  
32  
33  
34  
35  
36  
37  
38  
39  
40  
41  
42  
43  
44

45 Preliminary experiments conducted on our medium model of pathological plasma showed that a PLL  
46 coating successfully prevented beads from deteriorating. We analysed the physical/mechanical  
47 characteristics of the biomaterial with and without a PLL coating. Looking at the morphology, we  
48 observed an immediate and stable reduction of about 20 % in the beads' diameter after a PLL coating  
49 was applied, without any significant impact on cell viability. Analysis of the distribution of PLL  
50 showed that it was not able to enter the core of the alginate bead, remaining only on its shell. This  
51 phenomenon was also reported by Yahia et al. (Tam et al., 2011). In addition, the presence of the  
52 coating significantly increased the elastic modulus of the external area of the beads, making them  
53  
54  
55  
56  
57  
58  
59  
60

1  
2  
3 resistant to deterioration. Regarding the porosity, we did not notice any measurable difference between  
4 beads with or without a PLL coating. Both conditions had a cut-off between 41 and 103nm.

5  
6  
7 Fluorescent albumin, IgG, and nanoparticles of 41nm in diameter could effectively enter the beads,  
8 after 24 hours' incubation, but they were impermeable to polystyrene nanoparticles of 103nm, as also  
9 observed by Tran et al. (Tran et al., 2014). Of note, some large molecules physiologically produced by  
10 hepatocytes fell within this cut-off value (such as fibrinogen, about 48nm in hydrodynamic diameter  
11 (Bratek-Skicki, Zeliszewska, & Ruso, 2016)) and their transfer between the polymer network and the  
12 surrounding medium could be hindered. Importantly, considering that liver sinusoidal endothelial cells  
13 (the cells that delimit the space of Disse together with hepatocytes, controlling the trafficking of  
14 macromolecules), have fenestrae with diameter between 50-300nm (Wisse, 2002), the cut-off of our  
15 beads fitted well with this physiological range. On the basis of our results, we concluded that a large  
16 set of molecules produced by the encapsulated hepatocytes (and those present in the culture medium)  
17 could leave (and enter) the alginate matrix, an essential factor for BAL therapy.

18  
19  
20 We then evaluated whether or not the presence of this additional polymer could affect the cells'  
21 metabolic performance. According to our observations, encapsulated cell viability was affected neither  
22 by the long-term culture of cells nor by the presence of PLL. Noticeably, one of the markers of liver  
23 cell functionality is albumin production. Monitoring this secretion between the two conditions (with or  
24 without PLL) in shaken conditions showed a progressive increase throughout the culture up to day 14  
25 with an advantage for PLL coated beads, corresponding to efficient HepaRG differentiation. On day  
26 14, we tested different metabolic activities required for BAL applications, such as ammonia and  
27 lactate elimination. We were not able to measure any significant difference between either condition,  
28 with the exception of a downward trend in xenobiotic activities, and more precisely for CYP1A1/2,  
29 when the coating was present. This might be due to an increase in the beads' core stiffness after  
30 shrinking. Chen et al. (Chen, Khetani, Lee, Bhatia, & Van Vliet, 2009) effectively cultured rat  
31 hepatocytes on polyelectrolyte multilayers and found that albumin production and CYP1A activity  
32 decreased with increasing substrate stiffness.

33  
34  
35  
36  
37  
38  
39  
40  
41  
42  
43  
44  
45  
46  
47  
48  
49  
50  
51  
52  
53  
54  
55  
56  
57  
58  
59  
60

1  
2  
3 In the next step, we tested the functionality of cells on an equivalent pathological plasma medium,  
4 reproducing clinical therapy. We estimated that this biomass (alginate-PLL encapsulated HepaRG)  
5 had the characteristics necessary for extracorporeal BAL application. To support this hypothesis, we  
6 decided to use it in the PDB, compatible with the system developed in our laboratory (Figaro, Pereira,  
7 Rada, et al., 2015). Similar bioreactor designs, such as stirred-tank bioreactors, have long been used in  
8 large-scale culture of mammalian cells to provide an environment allowing control of oxygen, pH, and  
9 the continuous addition and removal of medium. They are commonly used for the large-scale  
10 production of spheroids that can be maintained for extended periods (Tostões et al., 2012), classically  
11 used in toxicological applications (Rebello et al., 2015). Moreover, Dr. Nyberg's group, who recently  
12 proved the beneficial role of the spheroid-reservoir BAL in treating pigs experiencing  
13 posthepatectomy ALF (Chen HS., Joo DJ., Shaheen M., Li Y., Wang Y., Yang J., Nicolas CT.,  
14 Predmore K., Amiot B., Michalak G., Mounajjed T., Fidler J., Kremers WK., 2019), highlighted how  
15 an impeller-agitated bioreactor could support high volumes of hepatocyte spheroid solutions, with a  
16 simple and compact design that is easy to scale up for BAL clinical applications (McIntosh, Corner,  
17 Amiot, & Nyberg, 2009). Overall, we consider that the PDB hosting alginate-PLL encapsulated  
18 HepaRG fitted these important criteria and, to our knowledge, it is the first time that this design has  
19 been used for BAL applications.

20  
21  
22  
23  
24  
25  
26  
27  
28  
29  
30  
31  
32  
33  
34  
35  
36  
37  
38  
39  
40 HepaRG matured in PLL alginate beads were able to produce proteins, detoxify ammonia and  
41 metabolize lactate to levels comparable or superior to other published works with similar cells  
42 (Nibourg et al., 2013) or primary porcine hepatocytes in the AMC-BAL (Poyck et al., 2007). The  
43 latter two activities were superior in the PDB compared to the shaken conditions setup linked with net  
44 cellular activity, as the results were normalized by the controls with empty alginate-PLL beads. It is  
45 difficult to assume that the perfusion of medium was the key element for the enhanced activity  
46 observed in PDB, given the very low perfusion flow in our experiments. We thus hypothesized that  
47 such improvement was promoted by increased oxygenation of the culture medium. The latter is  
48 associated with the synergistic role of orbital shaking culture and the increased exchange surface  
49 between the medium and the external environment in PDB rather than the shaken setup. Adam et al.  
50  
51  
52  
53  
54  
55  
56  
57  
58  
59  
60

1  
2  
3 assumed that improved oxygenation when cultivating HepaRG cells under shaking conditions would  
4 lead to mitochondrial biogenesis, improving hepatic differentiation and cell metabolic activity (such as  
5 ammonia detoxification and CYP-3A4 activity) (Adam et al., 2018). In addition, the role of oxygen on  
6 HepaRG differentiation and functions is crucial, as observed by van Wenum et al., where the authors  
7 demonstrated that culturing HepaRG in hyperoxia (i.e. 40 % O<sub>2</sub>) enhanced cell differentiation and  
8 improved metabolic functions (such as ammonia detoxification and CYP3A4 activity), when  
9 compared with normoxia conditions (i.e. 21 % O<sub>2</sub>) (van Wenum et al., 2018).  
10  
11  
12  
13  
14  
15  
16  
17  
18

19 In PDB, we noticed a significant decrease of around 40 % in initial ammonia concentrations and  
20 around 30 % in lactate after 6 hours of cell perfusion in the equivalent pathological plasma medium.  
21 At the end of the experiment, we did not notice any deterioration of the alginate-PLL beads or loss of  
22 cells, observing the supernatant on bright field microscopy. This feature, together with the presence of  
23 filters that avoid cells escaping from the bioreactor, is of key importance for conducting safe treatment  
24 for the patient.  
25  
26  
27  
28  
29  
30

### 31 **5. Conclusion**

32  
33 We adapted the HepaRG biomass encapsulated in alginate beads to the conditions of ALF therapy by  
34 adding a PLL coating. This coating covered the shell of the beads without altering the porosity or  
35 viability of the cells. In terms of metabolic activity, we measured very interesting performances in line  
36 with those required of BAL in the treatment of ALF. The next step will be to implement the PDB in  
37 the BAL, currently being optimized in our laboratory, and start the preclinical experiments on rodent  
38 ALF models.  
39  
40  
41  
42  
43  
44  
45

### 46 **6. Acknowledgement**

47  
48 We thank Dr Antonietta Messina and Dr Anne Dubart-Kupperschmitt (INSERM U1193) for the  
49 fruitful discussion throughout this work, and Augustin Lerebours, for his technical assistance.  
50

51  
52 The HepaRG cell line, media and supplements used were supported by Biopredic International  
53 (funded by ANR 16-RHUS-0005 in the framework of the iLite programme), for which the authors  
54 express their appreciation. This cell line was patented by Inserm under number WO 03/004627.  
55  
56  
57  
58  
59  
60

## 7. References

- Adam, A. A. A., van der Mark, V. A., Donkers, J. M., Wildenberg, M. E., Oude Elferink, R. P. J., Chamuleau, R. A. F. M., & Hoekstra, R. (2018). A practice-changing culture method relying on shaking substantially increases mitochondrial energy metabolism and functionality of human liver cell lines. *PLoS ONE*, *13*(4), 1–19. <https://doi.org/10.1371/journal.pone.0193664>
- Benson, J. P., Papas, K. K., Constantinidis, I., & Sambanis, A. (1997). Towards the development of a bioartificial pancreas: Effects of poly-L- lysine on alginate beads with BTC3 cells. *Cell Transplantation*, *6*(4), 395–402. [https://doi.org/10.1016/s0963-6897\(97\)00044-4](https://doi.org/10.1016/s0963-6897(97)00044-4)
- Bhujbal, S. V., Paredes-Juarez, G. A., Niclou, S. P., & de Vos, P. (2014). Factors influencing the mechanical stability of alginate beads applicable for immunoisolation of mammalian cells. *Journal of the Mechanical Behavior of Biomedical Materials*, *37*, 196–208. <https://doi.org/10.1016/j.jmbbm.2014.05.020>
- Bratek-Skicki, A., Zeliszewska, P., & Ruso, J. M. (2016). Fibrinogen: A journey into biotechnology. *Soft Matter*, *12*(42), 8393–8653. <https://doi.org/10.1039/C6SM01895E>
- Capone, S. H., Dufresne, M., Rechel, M., Fleury, M. J., Salsac, A. V., Paullier, P., ... Legallais, C. (2013). Impact of Alginate Composition: From Bead Mechanical Properties to Encapsulated HepG2/C3A Cell Activities for In Vivo Implantation. *PLoS ONE*, *8*(4). <https://doi.org/10.1371/journal.pone.0062032>
- Catapano, G., Gerlach, J. C. (2007). *Bioreactors for liver tissue engineering*. (R. R. & E. C. N Ashammakhi, Ed.), *Topics in tissue engineering*. Oulu, Finland: Oulu University.
- Cerec, V., Glaise, D., Garnier, D., Morosan, S., Turlin, B., Drenou, B., ... Corlu, A. (2007). Transdifferentiation of hepatocyte-like cells from the human hepatoma hepaRG cell line through bipotent progenitor. *Hepatology*, *45*(4), 957–967. <https://doi.org/10.1002/hep.21536>
- Chen, A. A., Khetani, S. R., Lee, S., Bhatia, S. N., & Van Vliet, K. J. (2009). Modulation of hepatocyte phenotype in vitro via chemomechanical tuning of polyelectrolyte multilayers. *Biomaterials*, *30*(6), 1113–1120. <https://doi.org/10.1016/j.biomaterials.2008.10.055>
- Chen HS., Joo DJ., Shaheen M., Li Y., Wang Y., Yang J., Nicolas CT., Predmore K., Amiot B., Michalak G., Mounajjed T., Fidler J., Kremers WK., N. S. (2019). Randomized Trial of Spheroid Reservoir

- 1  
2  
3 Bioartificial Liver in Porcine Model of Posthepatectomy Liver Failure. *Hepatology*, 69(1), 329–  
4 342. <https://doi.org/10.1002/hep.30184>  
5  
6  
7 Cusin, F., Azevedo, L. F., Bonnaventure, P., Desmeules, J., Daali, Y., & Pastor, C. M. (2017).  
8 Hepatocyte Concentrations of Indocyanine Green Reflect Transfer Rates Across Membrane  
9 Transporters, 171–178. <https://doi.org/10.1111/bcpt.12671>  
10  
11  
12 De Vos, P., De Haan, B., & Van Schilfgaarde, R. (1997). Effect of the alginate composition on the  
13 biocompatibility of alginate-polylysine microcapsules. *Biomaterials*, 18(3), 273–278.  
14  
15  
16 [https://doi.org/10.1016/s0142-9612\(96\)00135-4](https://doi.org/10.1016/s0142-9612(96)00135-4)  
17  
18  
19 Diaz, G. J. (2000). Basolateral and canalicular transport of xenobiotics in the hepatocyte: A review.  
20  
21 *Cytotechnology*, 34(3), 225–236. <https://doi.org/10.1023/A:1008152205697>  
22  
23  
24 Doré, E., & Legallais, C. (1999). A new concept of bioartificial liver based on a fluidized bed bioreactor.  
25  
26 *Therapeutic Apheresis*, 3(3), 264–267. <https://doi.org/10.1046/j.1526-0968.1999.00152.x>  
27  
28  
29 Du, J., & Yarema, K. J. (2014). Cell Microencapsulation for Tissue Engineering and Regenerative  
30  
31 Medicine. *Micro-and Nanoengineering of the Cell Surface*, 23, 215–239.  
32  
33 <https://doi.org/10.1016/B978-1-4557-3146-6.00010-6>  
34  
35  
36 Dusseault, J., Leblond, F. A., Robitaille, R., Jourdan, G., Tessier, J., Ménard, M., ... Hallé, J. P. (2005).  
37  
38 Microencapsulation of living cells in semi-permeable membranes with covalently cross-linked  
39  
40 layers. *Biomaterials*, 26(13), 1515–1522. <https://doi.org/10.1016/j.biomaterials.2004.05.013>  
41  
42  
43 Edwards-Lévy, F., & Lévy, M. C. (1999). Serum albumin-alginate coated beads: Mechanical properties  
44  
45 and stability. *Biomaterials*, 20(21), 2069–2084. [https://doi.org/10.1016/s0142-9612\(99\)00111-8](https://doi.org/10.1016/s0142-9612(99)00111-8)  
46  
47  
48 Elkayam, T., Amitay-Shaprut, S., Dvir-Ginzberg, M., Harel, T., & Cohen, S. (2006). Enhancing the drug  
49  
50 metabolism activities of C3A -a human hepatocyte cell line- by tissue engineering within alginate  
51  
52 scaffolds. *Tissue Engineering*, 12(5), 1357–1368. <https://doi.org/10.1089/ten.2006.12.1357>  
53  
54  
55 Figaro, S., Pereira, U., Dumé, A. S., Rada, H., Capone, S., Bengrine, A., ... Legallais, C. (2015).  
56  
57 SUPPLIVER: Bioartificial supply for liver failure. *Irbm*, 36(2), 101–109.  
58  
59 <https://doi.org/10.1016/j.irbm.2015.01.010>  
60  
61  
62 Figaro, S., Pereira, U., Rada, H., Semenzato, N., Pouchoulin, D., & Legallais, C. (2015). Development  
63  
64 and validation of a bioartificial liver device with fluidized bed bioreactors hosting alginate-

- 1  
2  
3 encapsulated hepatocyte spheroids. *Proceedings of the Annual International Conference of the*  
4 *IEEE Engineering in Medicine and Biology Society, EMBS*, 1335–1338.  
5  
6 <https://doi.org/10.1109/EMBC.2015.7318615>  
7  
8  
9 Gagnon, P., Nian, R., Leong, D., & Hoi, A. (2015). Transient conformational modification of  
10 immunoglobulin G during purification by protein A affinity chromatography. *Journal of*  
11 *Chromatography A*, 1395, 136–142. <https://doi.org/10.1016/j.chroma.2015.03.080>  
12  
13  
14 Gautier, A., Carpentier, B., Dufresne, M., Vu Dinh, Q., Paullier, P., & Legallais, C. (2011). Impact of  
15 alginate type and bead diameter on mass transfers and the metabolic activities of encapsulated c3a  
16 cells in bioartificial liver applications. *European Cells and Materials*, 21(0), 94–106.  
17  
18 <https://doi.org/10.22203/ecm.v021a08>  
19  
20  
21 Goosen, M. F. A., O'Shea, G. M., Gharapetian, H. M., Chou, S., & Sun, A. M. (1985). Optimization of  
22 microencapsulation parameters: Semipermeable microcapsules as a bioartificial pancreas.  
23 *Biotechnology and Bioengineering*, 27(2), 146–150. <https://doi.org/10.1002/bit.260270207>  
24  
25  
26 Graaf, W. De, Häusler, S., Heger, M., Ginhoven, T. M. Van, Cappellen, G. Van, Bennink, R. J., ...  
27 Stieger, B. (2011). Transporters involved in the hepatic uptake of and indocyanine green Tc-  
28 mebrotfenin. *Journal of Hepatology*, 54(4), 738–745. <https://doi.org/10.1016/j.jhep.2010.07.047>  
29  
30  
31 Joly, A., Desjardins, J.-F., Fremond, B., Desille, M., Campion, J.-P., Malledant, Y., ... Clement, B.  
32 (1997). Survival, proliferation, and functions of porcine hepatocytes encapsulated in coated  
33 alginate beads: a step toward a reliable bioartificial liver. *Transplantation*, 63(6), 795–803.  
34  
35 <https://doi.org/10.1097/00007890-199703270-00002>  
36  
37  
38 Kandiah, P. A., & Subramanian, R. M. (2019). Extracorporeal devices. *Critical Care Clinics*, 35(1),  
39 135–150. <https://doi.org/10.1016/j.ccc.2018.08.003>  
40  
41  
42 Keefe, E. B. (2005). Acute liver failure. *Revista de Gastroenterología de México*, 70(1), 56–62.  
43  
44  
45 Khanna, O., Larson, J. C., Moya, M. L., Opara, E. C., & Brey, E. M. (2012). Generation of alginate  
46 microspheres for biomedical applications. *Journal of Visualized Experiments*, (66), 1–5.  
47  
48 <https://doi.org/10.3791/3388>  
49  
50  
51 Li, Y., Yang, G., & Mei, Z. (2012). Spectroscopic and dynamic light scattering studies of the interaction  
52 between pterodonic acid and bovine serum albumin. *Acta Pharmaceutica Sinica B*, 2(1), 53–59.  
53  
54  
55  
56  
57  
58  
59  
60

1  
2  
3 <https://doi.org/10.1016/j.apsb.2011.12.001>

4  
5 Lou, R., Yu, W., Song, Y., Ren, Y., Zheng, H., Guo, X., ... Ma, X. (2017). Fabrication of stable  
6 galactosylated alginate microcapsules via covalent coupling onto hydroxyl groups for hepatocytes  
7 applications. *Carbohydrate Polymers*, *155*, 456–465.

8  
9  
10 <https://doi.org/10.1016/j.carbpol.2016.08.098>

11  
12  
13 McIntosh, M. B., Corner, S. M., Amiot, B. P., & Nyberg, S. L. (2009). Engineering analysis and  
14 development of the spheroid reservoir bioartificial liver. *Proceedings of the 31st Annual*  
15 *International Conference of the IEEE Engineering in Medicine and Biology Society: Engineering*  
16 *the Future of Biomedicine, EMBC*, 5985–5988. <https://doi.org/10.1109/IEMBS.2009.5334687>

17  
18  
19  
20  
21  
22 Nibourg, G. A. A., Hoekstra, R., Hoeven, T. V. V. Der, Ackermans, M. T., Hakvoort, T. B. M., Gulik,  
23 T. M. V., & Chamuleau, R. A. F. M. (2013). Increased hepatic functionality of the human hepatoma  
24 cell line HeparG cultured in the AMC bioreactor. *International Journal of Biochemistry and Cell*  
25 *Biology*, *45*(8), 1860–1868. <https://doi.org/10.1016/j.biocel.2013.05.038>

26  
27  
28  
29  
30  
31 Pasqua, M., Pereira, U., Messina, A., de Lartigue, C., Vigneron, P., Dubart-Kupperschmitt, A., &  
32 Legallais, C. (2020). HeparG Self-Assembled Spheroids in Alginate Beads Meet the Clinical  
33 Needs for Bioartificial Liver. *Tissue Engineering Part A*, ahead of p, 1–33.  
34  
35 <https://doi.org/10.1089/ten.tea.2019.0262>

36  
37  
38  
39 Poyck, P. P. C., Hoekstra, R., van Wijk, A. C. W. A., Attanasio, C., Calise, F., Chamuleau, R. A. F. M.,  
40 & van Gulik, T. M. (2007). Functional and morphological comparison of three primary liver cell  
41 types cultured in the AMC bioartificial live. *Liver Transplantation*, *13*(4), 589–598.  
42  
43 <https://doi.org/10.1002/lt.21090>

44  
45  
46  
47 Rebelo, S. P., Costa, R., Estrada, M., Shevchenko, V., Brito, C., & Alves, P. M. (2015). HeparG  
48 microencapsulated spheroids in DMSO-free culture: novel culturing approaches for enhanced  
49 xenobiotic and biosynthetic metabolism. *Archives of Toxicology*, *89*(8), 1347–1358.  
50  
51 <https://doi.org/10.1007/s00204-014-1320-9>

52  
53  
54  
55  
56 Selden, C., Bundy, J., Erro, E., Puschmann, E., Miller, M., Kahn, D., ... Spearman, C. W. (2017). A  
57 clinical-scale BioArtificial Liver, developed for GMP, improved clinical parameters of liver  
58 function in porcine liver failure. *Scientific Reports*, *7*(1), 1–19. <https://doi.org/10.1038/s41598->  
59  
60

017-15021-4

- 1  
2  
3  
4  
5 Simó, G., Fernández-Fernández, E., Vila-Crespo, J., Ruipérez, V., & Rodríguez-Nogales, J. M. (2017).  
6  
7 Research progress in coating techniques of alginate gel polymer for cell encapsulation.  
8  
9 *Carbohydrate Polymers*, 170, 1–14. <https://doi.org/10.1016/j.carbpol.2017.04.013>  
10  
11 Strand, B. L., Ryan, L., In't Veld, P., Kulseng, B., Rokstad, A. M., Skjåk-Bræk, G., & Espevik, T.  
12  
13 (2001). Poly-L-lysine induces fibrosis on alginate microcapsules via the induction of cytokines.  
14  
15 *Cell Transplantation*, 10(3), 263–275. <https://doi.org/10.3727/000000001783986800>  
16  
17 Strand, Berit L., Coron, A. E., & Skjak-Braek, G. (2017). Current and future perspectives on alginate  
18  
19 encapsulated pancreatic islet. *Stem Cells Translational Medicine*, 6(4), 1053–1058.  
20  
21 <https://doi.org/10.1002/sctm.16-0116>  
22  
23 Tam, S. K., Bilodeau, S., Dusseault, J., Langlois, G., Hallé, J. P., & Yahia, L. H. (2011).  
24  
25 Biocompatibility and physicochemical characteristics of alginate-polycation microcapsules. *Acta*  
26  
27 *Biomaterialia*, 7(4), 1683–1692. <https://doi.org/10.1016/j.actbio.2010.12.006>  
28  
29 Tostões, R. M., Leite, S. B., Serra, M., Jensen, J., Björquist, P., Carrondo, M. J. T., ... Alves, P. M.  
30  
31 (2012). Human liver cell spheroids in extended perfusion bioreactor culture for repeated-dose drug  
32  
33 testing. *Hepatology*, 55(4), 1227–1236. <https://doi.org/10.1002/hep.24760>  
34  
35 Tran, N. M., Dufresne, M., Helle, F., Hoffmann, T. W., Francois, C., Brochot, E., ... Castelain, S.  
36  
37 (2014). Alginate hydrogel protects encapsulated hepatic HuH-7 cells against hepatitis C virus and  
38  
39 other viral infections. *PLoS ONE*, 9(10), 16–17. <https://doi.org/10.1371/journal.pone.0109969>  
40  
41 Van De Kerkhove, M. P., Poyck, P. P. C., Deurholt, T., Hoekstra, R., Chamuleau, R. A. F. M., & Van  
42  
43 Gulik, T. M. (2005). Liver support therapy: An overview of the AMC-bioartificial liver research.  
44  
45 *Digestive Surgery*, 22(4), 254–264. <https://doi.org/10.1159/000088055>  
46  
47 van Wenum, M., Adam, A. A. A., van der Mark, V. A., Chang, J. C., Wildenberg, M. E., Hendriks, E.  
48  
49 J., ... Hoekstra, R. (2018). Oxygen drives hepatocyte differentiation and phenotype stability in  
50  
51 liver cell lines. *Journal of Cell Communication and Signaling*, 12(3), 575–588.  
52  
53 <https://doi.org/10.1007/s12079-018-0456-4>  
54  
55 Van Wenum, M., Chamuleau, R. A., Van Gulik, T. M., Siliakus, A., Seppen, J., & Hoekstra, R. (2014).  
56  
57 Bioartificial livers in vitro and in vivo: Tailoring biocomponents to the expanding variety of  
58  
59  
60

1  
2  
3 applications. *Expert Opinion on Biological Therapy*, 14(12), 1745–1760.  
4  
5 <https://doi.org/10.1517/14712598.2014.950651>  
6

7 Wang, N., Adams, G., Buttery, L., Falcone, F. H., & Stolnik, S. (2009). Alginate encapsulation  
8 technology supports embryonic stem cells differentiation into insulin-producing cells. *Journal of*  
9 *Biotechnology*, 144(4), 304–312. <https://doi.org/10.1016/j.jbiotec.2009.08.008>  
10  
11  
12

13 Wisse, F. B. and E. (2002). Structural and functional aspects of liver sinusoidal endothelial cell  
14 fenestrae: a review. *Comp Hepatol*, 1(1). <https://doi.org/10.1186/1476-5926-1-1>  
15  
16

17 Zhou, P., Shao, L., Zhao, L., Lv, G., Pan, X., Zhang, A., ... Li, L. (2016). Efficacy of Fluidized Bed  
18 Bioartificial Liver in Treating Fulminant Hepatic Failure in Pigs: A Metabolomics Study. *Scientific*  
19 *Reports*, 6(1), 1–9. <https://doi.org/10.1038/srep26070>  
20  
21  
22  
23  
24  
25  
26  
27  
28  
29  
30  
31  
32  
33  
34  
35  
36  
37  
38  
39  
40  
41  
42  
43  
44  
45  
46  
47  
48  
49  
50  
51  
52  
53  
54  
55  
56  
57  
58  
59  
60

**Tables:**

Table 1: Fluorescent molecules with their characteristics used to investigate bead permeability.  $D_H$  indicates the hydrodynamic diameter of the protein without the fluorophore; MW indicates the molecular weight.

Fluorescent marker	Supplier	Molecular weight or size	Concentration	Reference
Albumin–fluorescein isothiocyanate (FITC)	Sigma-Aldrich	$D_H = 7.3$ nm (Li, Yang, & Mei, 2012); MW = 66 kDa	100 $\mu\text{g/mL}$ in WE medium at 37°C	(Wang, Adams, Buttery, Falcone, & Stolnik, 2009)
Alexa Fluor 488 conjugate IgG	Thermofisher	$D_H = 11.5$ nm (Gagnon, Nian, Leong, & Hoi, 2015); MW = 160 kDa	100 $\mu\text{g/mL}$ in WE medium at 37°C	(Tran et al., 2014)
Nanoparticles (NPs)	Estapor, Merk Chimie	41 nm 103 nm 249 nm	340 $\mu\text{g/mL}$ in WE medium at room temperature	(Tran et al., 2014)

Table 2: Media for metabolic characterization on day 14 post-encapsulation and tests performed.

	HepaRG proliferation culture medium	Test medium	Human equivalent pathological plasma medium
<b>Medium composition</b>	William's E medium + Biopredic 710 proliferation media	HepaRG proliferation culture medium + 1.5 mM ammonium chloride + 2 mM L-Lactate	HepaRG proliferation culture medium + 70 g/L bovine serum albumin + 1.5 mM ammonium chloride + 2 mM L-Lactate
<b>Metabolic performances tested</b>	Albumin synthesis rate (2 h)	Albumin synthesis rate (2 h)	Albumin synthesis rate (6 h)
<b>(Test duration)</b>	ICG clearance rate (1 h)	Ammonia detoxification rate (2 h)	Ammonia detoxification rate (6 h)
	CYP 1A1/2 activity (1 h)	Lactate clearance rate (2 h)	Lactate clearance rate (6 h)

Table 3: Summary of metabolic activities between biomass in alginate beads with and without a PLL coating. Activities tested on day 14 post-encapsulation in shaken conditions, in HepaRG proliferation culture medium, and in test medium.  $N > 3$

Biomass ( $5 \times 10^6$ cells)	HepaRG proliferation culture medium			Test medium		
	Albumin synthesis rate ( $\mu\text{g/h}/10^6$ )	ICG releasing rate ( $\mu\text{g/h}/10^6$ )	CYP 1A1/2 activity ( $\text{pmol/h}/10^6$ )	Albumin synthesis rate ( $\mu\text{g/h}/10^6$ )	Ammonia detoxification rate ( $\text{nmol/h}/10^6$ )	Lactate clearance rate ( $\text{nmol/h}/10^6$ )
Alginate beads without PLL coating	$0.85 \pm 0.42$	$45.3 \pm 6.9$	$6.5 \pm 1.9$	$0.43 \pm 0.19$	$90.4 \pm 61.0$	$111.8 \pm 68.3$
Alginate beads with PLL coating	$0.62 \pm 0.22$	$20.9 \pm 7.8$	$1.8 \pm 1.0$	$0.56 \pm 0.24$	$73.7 \pm 28.4$	$95.6 \pm 50.4$

1  
2  
3 **Figure 1.** A: Experimental setups allowing culture and metabolic characterization of the encapsulated  
4 biomass. Left: Shaken condition: Petri dish hosting  $5 \times 10^6$  cells in 7.5 mL of surrounding medium kept  
5 in continuous orbital shaking (60 rpm). Right: Perfused dynamic bioreactor (PDB): double arm glass  
6 flask hosting  $50 \times 10^6$  cells in 37.5 mL of total medium volume. The peristaltic pump (Ismatec) makes  
7 constant perfusion possible (flow rate = 0.4 mL/min) while the beads are kept in continuous orbital  
8 shaking (80 rpm). The needles for media recirculation are protected with a filter membrane to avoid  
9 biomass escaping from the PDB. Two outlets are dedicated to filtered air intake to preserve sterility and  
10 guarantee gas exchanges. B: Experimental setup. After 2D amplification, cells were encapsulated in  
11 alginate beads and then cultivated for 14 days. Cell culture evolution was monitored analysing cell  
12 viability (by Live/Dead staining on days 0, 1, 7, 14) and albumin synthesis rate (overnight between days  
13 0-1, 6-7, 9-10, 13-14). On day 14 post-encapsulation, cell performance was tested by means of metabolic  
14 and xenobiotic tests in different media (HepaRG proliferation culture medium, test medium, and  
15 pathological plasma medium).

16  
17  
18  
19  
20  
21  
22  
23  
24  
25  
26  
27  
28  
29  
30  
31  
32 **Figure 2.** A: Distribution of PLL-rhodamine (red staining) in empty beads in comparison with the  
33 negative control (without PLL coating). Images taken in confocal microscopy (left images), phase  
34 contrast (central) and merging the two (right). Scale bar: 100  $\mu\text{m}$ . B: Elastic modulus of the outer surface  
35 of empty beads with and without a PLL coating on day 14. With an indentation of 3  $\mu\text{m}$ , the sensor  
36 penetrated only into the PLL layer, when present. Significance was analysed using a Mann-Whitney  
37 Test. \*\*\* indicates  $p < 0.001$ . N = 10 per batch of beads.

38  
39  
40  
41  
42  
43  
44  
45  
46  
47 **Figure 3.** Permeability of empty beads (coated or not with PLL) to fluorescent markers (albumin, IgG,  
48 nanoparticles of different diameters). DH indicates the hydrodynamic diameter without the fluorophore;  
49  $\emptyset$  indicates the diameter of the nanoparticles (NPs). Incubation lasted 24 hours. Pictures taken after  
50 washing the beads in WE. Scale bar: 100  $\mu\text{m}$ .

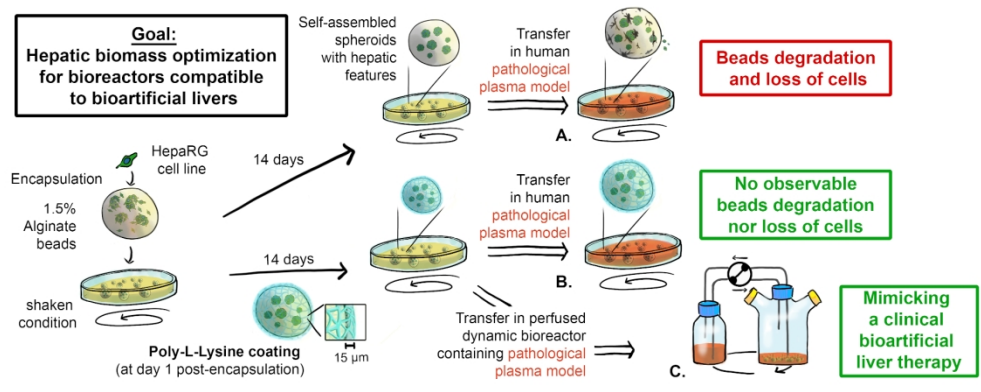
51  
52  
53  
54  
55  
56  
57 **Figure 4.** Observation of beads without and with PLL coating morphology by bright field microscopy  
58 (scale bar: 500  $\mu\text{m}$ ) and cell viability of alginate-PLL encapsulated cells (live/dead assay) by confocal  
59  
60

1  
2  
3 microscopy. In green (Calcein AM): viable cells, in red (ethidium homodimer-1): dead cells, in blue  
4  
5 (Hoechst 33342 dye): cell nuclei (scale bar 100  $\mu\text{m}$ ).  
6  
7  
8

9 **Figure 5.** Metabolic activities of cells in alginate-PLL beads, measured on day 14, over 6 hours'  
10 incubation in equivalent pathological plasma medium, in shaken conditions and a perfused dynamic  
11 bioreactor (PDB). A: albumin synthesis rate; B: ammonia detoxification rate; C: lactate detoxification  
12  
13  
14  
15 rate.  
16  
17  
18  
19  
20  
21  
22  
23  
24  
25  
26  
27  
28  
29  
30  
31  
32  
33  
34  
35  
36  
37  
38  
39  
40  
41  
42  
43  
44  
45  
46  
47  
48  
49  
50  
51  
52  
53  
54  
55  
56  
57  
58  
59  
60

For Peer Review

1  
2  
3  
4  
5  
6  
7  
8  
9  
10  
11  
12  
13  
14  
15  
16  
17  
18  
19  
20  
21  
22  
23  
24  
25  
26  
27  
28  
29  
30  
31  
32  
33  
34  
35  
36  
37  
38  
39  
40  
41  
42  
43  
44  
45  
46  
47  
48  
49  
50  
51  
52  
53  
54  
55  
56  
57  
58  
59  
60



Graphical abstract

168x67mm (300 x 300 DPI)

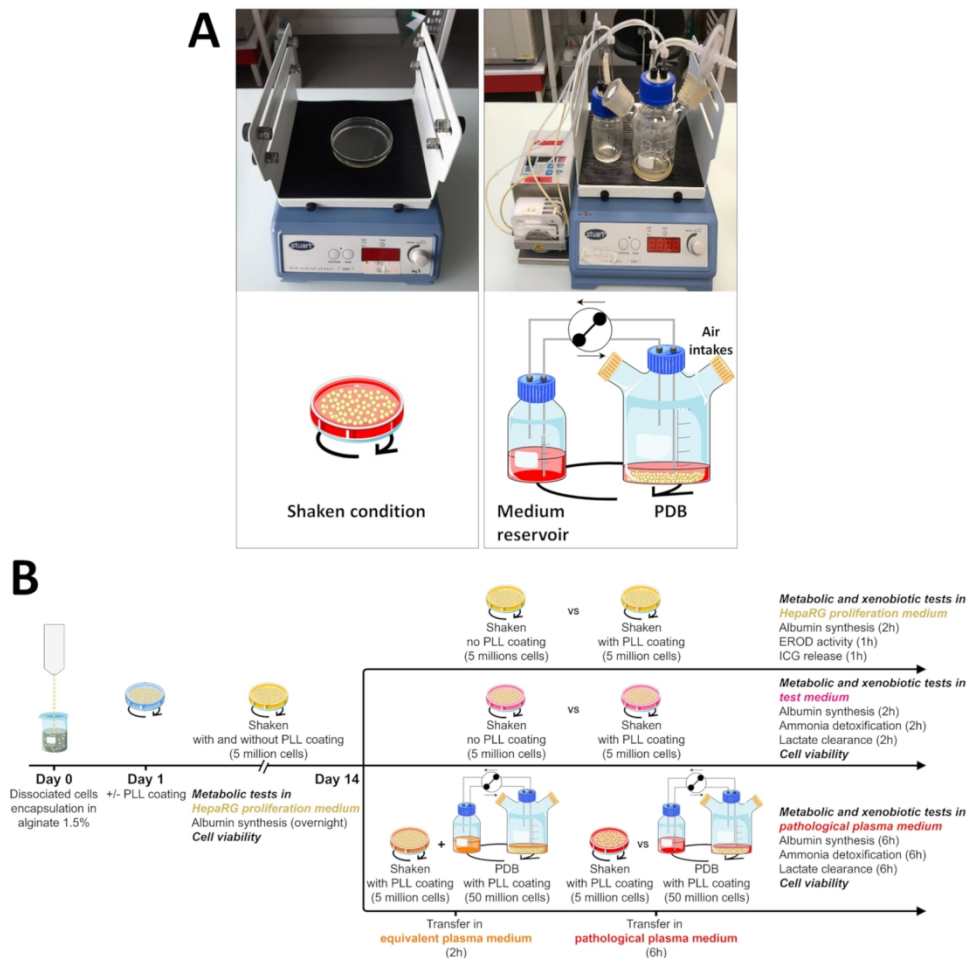


Figure 1. A: Experimental setups allowing culture and metabolic characterization of the encapsulated biomass. Left: Shaken condition: Petri dish hosting  $5 \times 10^6$  cells in 7.5 mL of surrounding medium kept in continuous orbital shaking (60 rpm). Right: Perfused dynamic bioreactor (PDB): double arm glass flask hosting  $50 \times 10^6$  cells in 37.5 mL of total medium volume. The peristaltic pump (Ismatec) makes constant perfusion possible (flow rate = 0.4 mL/min) while the beads are kept in continuous orbital shaking (80 rpm). The needles for media recirculation are protected with a filter membrane to avoid biomass escaping from the PDB. Two outlets are dedicated to filtered air intake to preserve sterility and guarantee gas exchanges. B: Experimental setup. After 2D amplification, cells were encapsulated in alginate beads and then cultivated for 14 days. Cell culture evolution was monitored analysing cell viability (by Live/Dead staining on days 0, 1, 7, 14) and albumin synthesis rate (overnight between days 0-1, 6-7, 9-10, 13-14). On day 14 post-encapsulation, cell performance was tested by means of metabolic and xenobiotic tests in different media (*HepaRG* proliferation culture medium, test medium, and pathological plasma medium).

149x146mm (300 x 300 DPI)

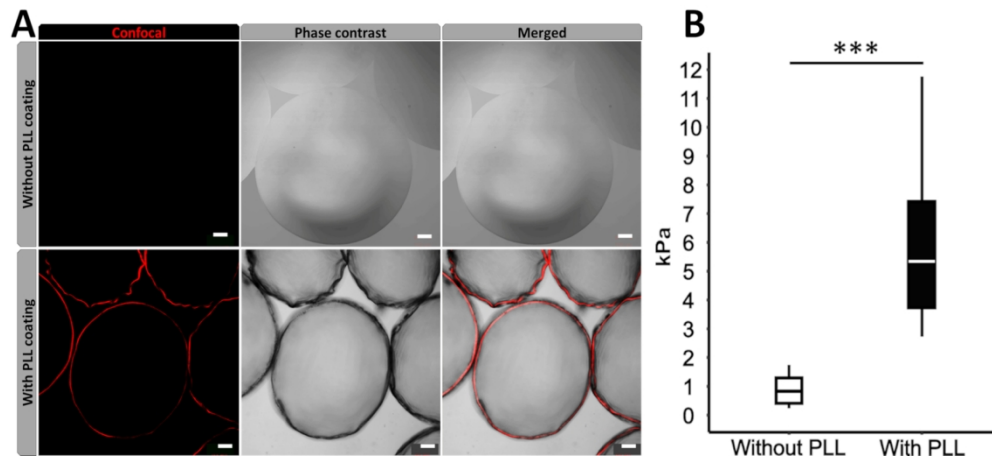


Figure 2. A: Distribution of PLL-rhodamine (red staining) in empty beads in comparison with the negative control (without PLL coating). Images taken in confocal microscopy (left images), phase contrast (central) and merging the two (right). Scale bar: 100  $\mu\text{m}$ . B: Elastic modulus of the outer surface of empty beads with and without a PLL coating on day 14. With an indentation of 3  $\mu\text{m}$ , the sensor penetrated only into the PLL layer, when present. Significance was analysed using a Mann-Whitney Test. \*\*\* indicates  $p < 0.001$ .  $N = 10$  per batch of beads.

149x67mm (300 x 300 DPI)

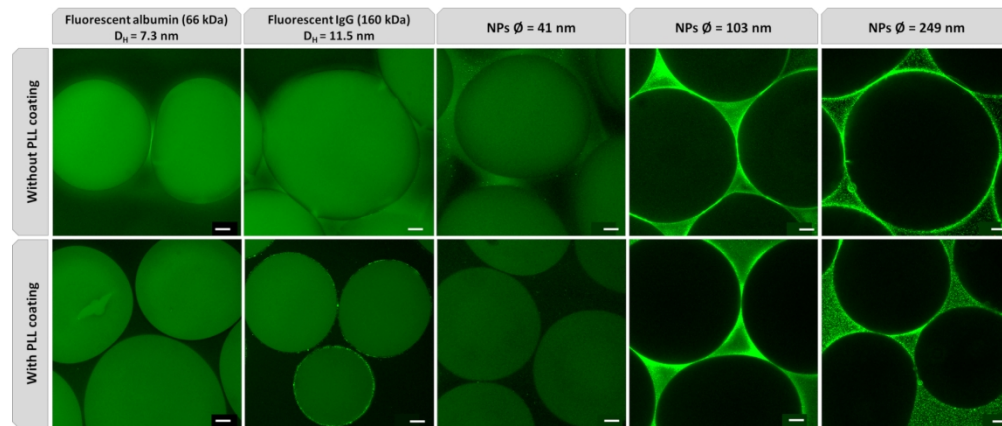


Figure 3. Permeability of empty beads (coated or not with PLL) to fluorescent markers (albumin, IgG, nanoparticles of different diameters).  $D_h$  indicates the hydrodynamic diameter without the fluorophore;  $\phi$  indicates the diameter of the nanoparticles (NPs). Incubation lasted 24 hours. Pictures taken after washing the beads in WE. Scale bar: 100  $\mu\text{m}$ .

159x68mm (300 x 300 DPI)

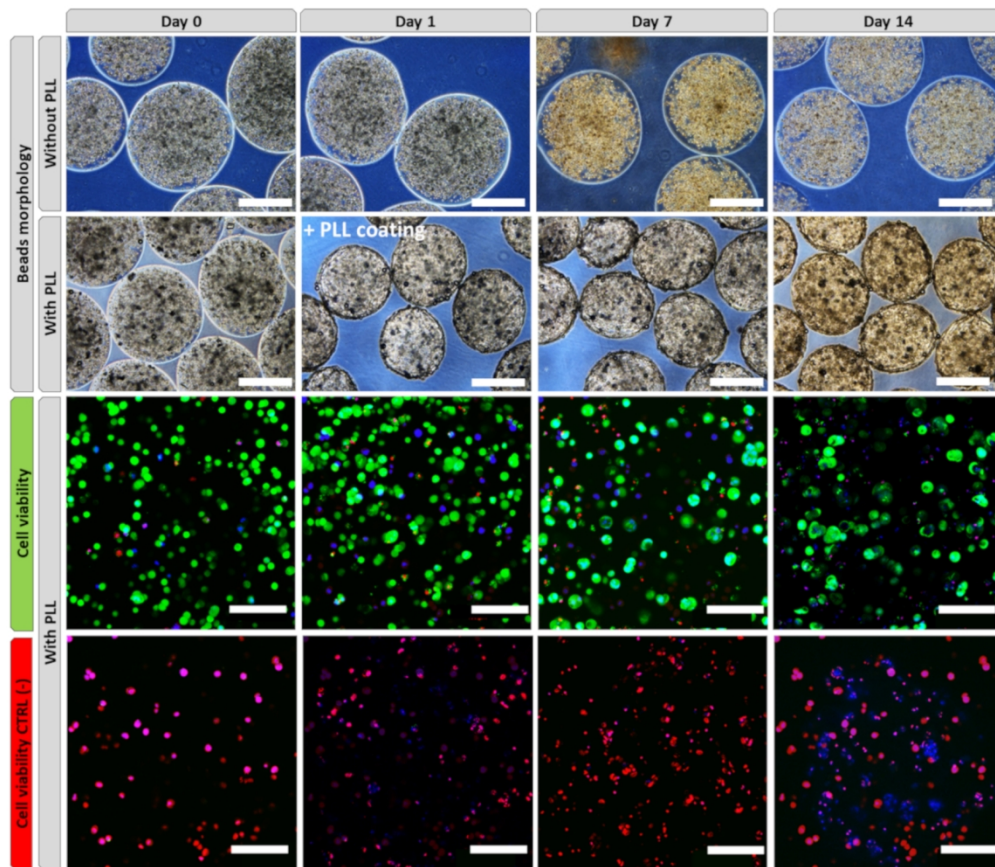


Figure 4. Observation of beads without and with PLL coating morphology by bright field microscopy (scale bar: 500 μm) and cell viability of alginate-PLL encapsulated cells (live/dead assay) by confocal microscopy. In green (Calcein AM): viable cells, in red (ethidium homodimer-1): dead cells, in blue (Hoechst 33342 dye): cell nuclei (scale bar 100 μm).

149x129mm (300 x 300 DPI)

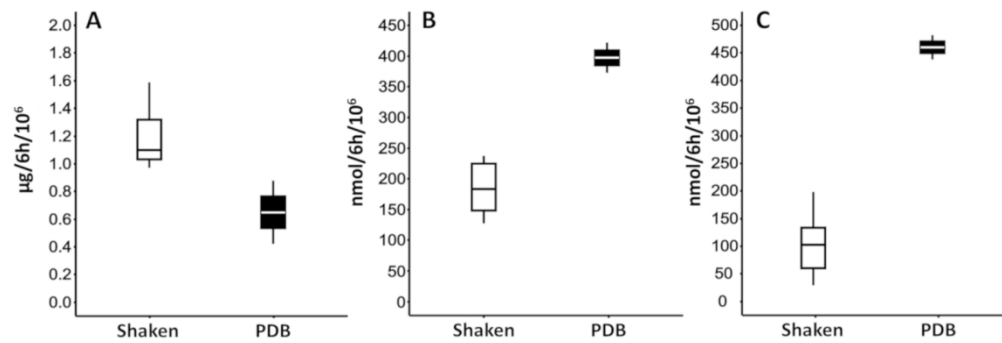
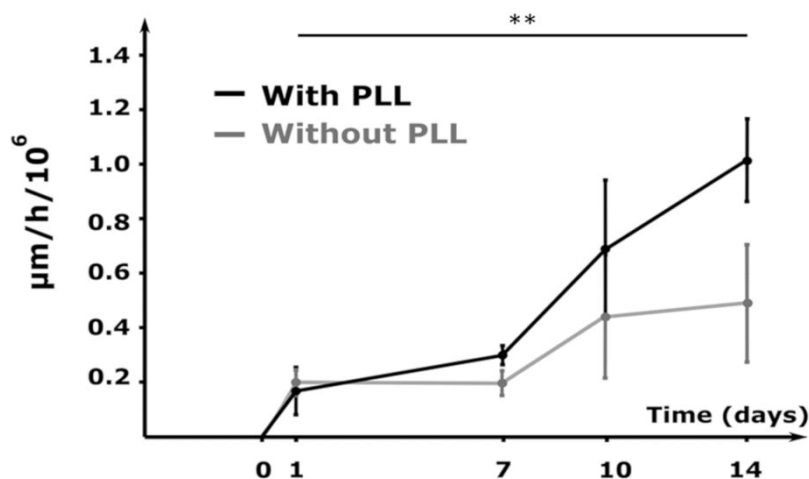


Figure 5. Metabolic activities of cells in alginate-PLL beads, measured on day 14, over 6 hours' incubation in equivalent pathological plasma medium, in shaken conditions and a perfused dynamic bioreactor (PDB). A: albumin synthesis rate; B: ammonia detoxification rate; C: lactate detoxification rate.

71x24mm (600 x 600 DPI)

**Figure 1, Supplementary Data.** Albumin secretion rate over time (overnight between days 0-1, 6-7, 9-10, 13-14) of encapsulated cells in alginate beads with and without PLL coating. For the condition with PLL, the increasing between day 1 and da14 was significant (\*\* indicates  $p < 0.01$ , significance analysed by Dunn's Multiple Comparisons Test).  $N > 3$ .



**Figure 2, Supplementary Data.** Cell viability (live/dead assay) of cells in alginate beads without and with PLL coating in shaken and PDB setups by confocal microscopy, after exposure to different culture media. In green (Calcein AM): viable cells, in red (ethidium homodimer-1): dead cells, in blue (Hoechst 33342 dye): cell nuclei. Scale bar: 100  $\mu\text{m}$ .

